THREE DIMENSIONAL RECONSTRUCTION WITH CONTRAST TRANSFER COMPENSATION FROM DEFOCUS SERIES

P.A. Penczek[1,2]*, J. Zhu[1], R. Schröder[3] and J. Frank[1,2]

[1]Wadsworth Center, New York State Department of Health, Albany, NY
[2]Department of Biomedical Sciences, School of Public Health, State University of New York at Albany, NY
[3]Department of Biophysics, Max-Planck Institute for Medical Research, Heidelberg, Germany

Abstract

Cryo-electron microscopy provides the means to quantitatively study macromolecules in their native state. However, the original mass distribution of the macromolecule is distorted by the contrast transfer function (CTF) of the electron microscope. In addition, the zeros of the CTF put a practical limit on the resolution that can be achieved. Substantial improvement to the quality of the results can be accomplished by collecting the data using a series of defocus settings. Such data sets can be combined and the resolution can be extended beyond the first zero of the CTF. This procedure can be applied either at the stage of raw data, or more effectively at the stage of reconstructed volumes which have a high signal-to-noise ratio as a result of averaging over many projections. A method of three-dimensional (3D) reconstruction that combines an algebraic, iterative 3D reconstruction technique with CTF correction is proposed. The potential to incorporate *a priori* knowledge into the reconstruction process is discussed. This approach was used to obtain a 3D reconstruction of the *E. coli* 70S ribosome from energy filtered cryo-images.

Key Words: Cryo-electron microscopy, energy filtered cryo-images, three-dimensional reconstruction, contrast transfer function correction.

*Address for correspondence:
P.A. Penczek
Wadsworth Center
New York State Department of Health
Empire State Plaza, P.O. Box 509
Albany, NY 12201-0509
Telephone number: (518) 474-4235
FAX number: (518) 486-2191
E-mail: pawel@wadsworth.org

Introduction

Single particle reconstruction methods [21] make it possible to obtain three-dimensional density maps of macromolecular complexes that are not amenable to crystallization. When combined with cryo techniques [8, 16, 28, 32] and recent advances in image processing methods [17, 18], these methods yield structural maps that can be quantitatively interpreted [9]. Even though substantial improvement in the resolution of three-dimensional results has been achieved, further progress is hampered by the image/contrast distortions introduced by the electron microscope (EM). These effects can be described within a linear, weak-phase approximation by the contrast transfer function (CTF) of the microscope. Additional distortions are caused by the inelastically scattered electrons which contribute a high and slowly varying background to the image. Moreover, if multiple scattering events occur, the inelastically scattered electrons can give rise to elastic bright field images, acting as "internal sources", and the image we observe can be thought of as a superposition of a large number of bright field images, each originating from an inelastically scattered electron having different angular incidence and energy [22]. The conventional linear contrast transfer function cannot account for these inelastic and multiple scattering effects. However, zero-loss energy filtering in the EM eliminates virtually all inelastically scattered electrons and thus reduces non-linear effects to a minimum. In ice, elastic scattering from nucleic acids is predicted to be more than twice as strong as from protein, whereas the amount of inelastic scattering is similar for the two types of molecules. Thus, energy filtration should also greatly increase the contrast between RNA and protein [26], a desired effect in the study of the protein-nucleic acid complexes such as the ribosome. Finally, by combining energy-filtered cryo-EM with CTF correction one can, in principle, obtain absolute densities of biological molecules that agree very well with those from X-ray structures [14, 25].

Linear Theory of the Contrast Transfer Function

The contrast transfer theory was formulated in the

seventies [4, 7, 11, 12, 15]. It can be demonstrated [29] that under the weak-phase approximation the relationship between the object and the bright field image can be described by the linear transfer theory. In Fourier space,

$$I(k) = H(k)\Phi(k) \tag{1}$$

where $\Phi(k)$ is the Fourier transform of the object (linearly related to the Coulomb potential distribution), $I(k)$ is the Fourier transform of the observed image, k is a vector in Fourier space related to the scattering angle θ by $k=\theta/\lambda$ (λ is the wavelength of the electrons), $k = |k|$, and $H(k)$ is the CTF and has the explicit form

$$H(k) = \sin \gamma(k) - W \cos\gamma(k) \tag{2}$$

The term W (here assumed to be constant in the spatial frequency range considered) is called *amplitude contrast ratio*, and $\gamma(k)$ is the phase shift produced by the lens aberrations and defocusing. $\gamma(k)$ is rotationally symmetric assuming that the astigmatism is negligible. In that case our CTF $H(k)$ is rotationally symmetric as well. The contrast transfer functions for our choice of defocus values are shown in Figure 1. Since the amplitude contrast is different for different atomic species, Equation 2 is strictly correct only for a single species of atoms [6, 10]. The use of single value for W implies that W will be to some extent specimen-dependent.

The presence of additional effects in the image formation process requires expansion of the CTF model given by Equation 2. These effects include: finite source size [7], energy spread [12, 30], resolution-limiting effects of the film [3], scanner [14], and drift [5, 13]. All these effects have a frequency-limiting impact on the EM image which can be approximately described by so called *envelope functions*. To demonstrate the effect of envelope functions, the same CTFs of Figure 1 are again shown for the conditions of our experiment (Fig. 2; for details see the section on Application to Energy-Filtered Images).

Methods of Correction for the CTF

The goal of the CTF correction (for a review of some of the earlier literature, see [27]) is to recover the original values of the amplitudes of the Fourier transform of the image, within the framework of the linear approximation.

According to Equation 1, Fourier transform of the observed image is the product of the CTF and the Fourier transform of the object. Thus, it is tempting to divide the Fourier transform by the CTF (estimated or known) to recover the exact values of the object:
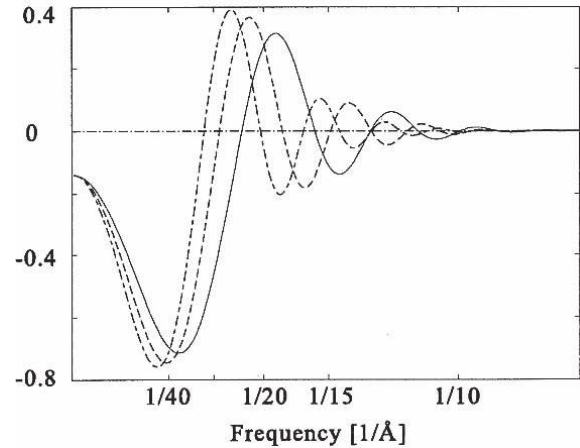
$$\Phi(k) \cong I(k) / H(k) \tag{3}$$

Figure 1. Theoretical contrast transfer function (eqn. 2) for three defocus values: 1.5 µm (_____), 2.0 µm (----), and 2.5 µm (-·--·-).
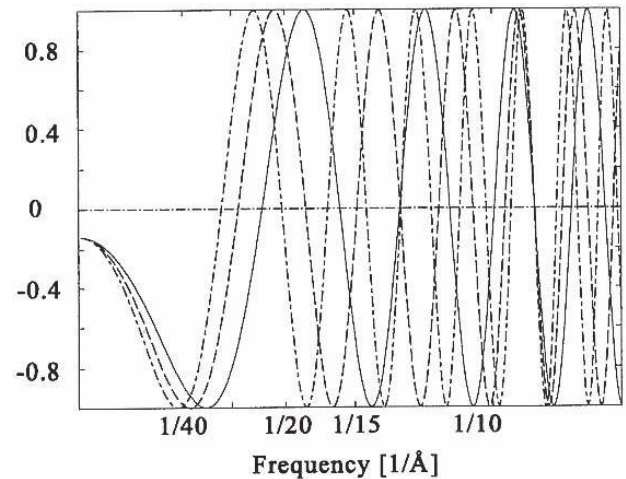

Figure 2. Theoretical contrast transfer function with envelope functions effects for three defocus values: 1.5 µm (_____), 2.0 µm (----), and 2.5 µm (-·--·-).

Unfortunately, this simple solution rarely yields desired results. In practice, the measured image is corrupted by noise, which will be enhanced upon division by the CTF in regions where the CTF is small. The CTF of the EM is low in the low-spatial frequency region, but also tends to zero at high spatial frequencies. Most problematic are zero crossings in the range between these extremes where division is impossible. Thus, a better approach is to take advantage of the fact that in most practical cases the noise is not correlated with the original image. Using this assumption one would seek a filter function $F(k)$ that minimizes the expected mean squared deviation of the restored object $\tilde{\Phi}(k) = F(k)I(k)$ from the original object [19]:

$$E[\,|\Phi(k) - F(k)I(k)|^2] \tag{4}$$

where $E[.]$ denotes the expectation over an ensemble of images. The solution to this problem is given by so-called *Wiener filter* [24]:

$$F(k) = \frac{H*(k)}{|H(k)|^2 + 1/SNR} \qquad (5)$$

Here SNR denotes the signal-to-noise ratio of original image and the noise (in the general case it can be frequency dependent and given by the ratio of the respective power spectra). In the noiseless case ($SNR \rightarrow \infty$) the Wiener filter approximates the pseudo-inverse filter [1] defined by:

$$F_{ps}(k) = \begin{cases} \dfrac{1}{H(k)} & H(k) \neq 0 \\ \\ for & \\ \\ 0 & H(k) = 0 \end{cases} \qquad (6)$$

Thus, it also approximates the simple inversion, as given by Equation 3. For the other extreme case, namely $SNR \rightarrow 0$, the application of the Wiener filter will approximately correspond to the multiplication by the CTF. In intermediate cases, depending on the value of the *SNR* used, the Wiener filter will in general amplify frequencies in those regions where CTF has moderate to large values and suppress frequencies in regions where the CTF has small values. In addition, as follows from Equation 5, wherever the CTF has zero value the filtered image will have its Fourier amplitude set to zero. Thus, the Wiener filtration does not make any attempts to recover the information in the missing frequency regions, a property that limits its appeal as a tool for the CTF correction for EM data. Moreover, the Wiener filters are often criticized for excessive suppression of the measurement noise, while performing only minor corrections [2].

The iterative methods for the CTF corrections [2] attempt to find an approximation $\tilde{\phi}(x)$ of an original image such that the squared residual error is minimized over the appropriate region of support:

$$|i(x) - h(x)*\tilde{\phi}(x)|^2 \rightarrow min \qquad (7)$$

Equation 7 is given in real space and * denotes convolution. The solution is found in a recursive manner starting from the initial approximation $\tilde{\phi}^{(0)}(x)$ (usually a blank image). The advantage of the iterative methods is that additional constraints can be incorporated into the process, either linear, in form of regularization, or non-linear, for example, as a positivity constraint. In some cases these additional constraints, often referred to as *a priori* knowledge of the image, can help to recover information suppressed by the zeros of the CTF.

The presence of zeros in the CTF of the electron microscope and the dependence of the locations of these zeros on the defocus value suggest that the CTF correction can be augmented by collecting a defocus series data set. Such data, if combined in Fourier space, should for all the practical purposes cover the whole range of frequencies. Assuming that L defocus values Δz_l have been used, both the Wiener filter method and iterative methods can be used to combine the data sets and correct for the CTF effects. The Wiener filter for the *l'th* data set has the form [10]:

$$F_l(k) = \frac{H_l^*(k)}{\sum_{l=1}^{L} |H_l(k)|^2 + 1/SNR} \qquad (8)$$

and the Fourier transform of the CTF corrected object is given by

$$\tilde{\Phi}(k) = \sum_{l=1}^{L} F_l(k) I_l(k) \qquad (9)$$

As in the case of a single defocus data set (Eqn. 5), the spatial frequency regions corresponding to the zeros of the CTFs are set to zero in the respective data sets. Thus, it becomes evident that the knowledge about the precise settings of the defocus during data collection is essential for this method to succeed.

The iterative method can be easily extended to the defocus case series by having Equation 7 modified to

$$\sum_{l=1}^{L} w_l |i(x) - h_l(x)*\tilde{\phi}_l(x)|^2 \rightarrow min \qquad (10)$$

where $w_l > 0$ defines the relative importance of the *l'th* defocus data set. As in the case of a single defocus data set (Eqn. 7) the solution is found in a recursive manner starting from the appropriate approximations $\tilde{\phi}_l^{(0)}(x)$ and the *a priori* knowledge about the original image can be easily incorporated.

In the field of electron microscopy the data are available in the form of projections of the biological macromolecule. Thus, in principle, the CTF correction should be applied directly to the 2D data (i.e., original micrographs). Unfortunately, due to the very low signal-to-noise ratio in cryo-EM images this method is not likely to succeed. Instead, the CTF correction has been applied after all the orientation parameters were found and a 3D reconstruction could be calculated. At this point, due to the heavy oversampling in Fourier space, the structure has much higher SNR, and errors in individual projections are less likely to dominate the result. Since our measured data are 2D projections of the structure, the best solution is to make CTF correction an integral part of the 3D

reconstruction procedure. In this way the final volume is obtained in one single step and any accumulation of errors is avoided.

To design the method of three-dimensional reconstruction with CTF compensation from defocus series, we have to modify Equation 10. Both 3D reconstruction and CTF application can be treated as algebraic problems. In real space, the effect of the CTF can be described by a point spread function, represented by a square matrix, and the projection operation by a non-square matrix P. Moreover, since the CTF function was assumed to be rotationally symmetric, it can be applied to the 3D object instead of 2D projections. Thus, denoting the unknown, CTF artifacts-free object by g and using matrix notation, we obtain from equation 10

$$(1-a)\sum_{l=1}^{L} w_l |d_l - P_l \hat{H}_l g|^2 + a|Bg|^2 \rightarrow \min \qquad (11)$$

where d is a vector containing all the available 2D projections, matrix B is a discrete approximation of the Laplacian and a is a Langrange multiplier. The value of a determines the relative smoothness of the solution g. This additional term will regularize the solution [20] and prevent adverse amplification of noise. The solution of Equation 11 is found using the steepest descent method [20]:

$$g^{(n+1)} = g^{(n)} + \lambda\{(1-a)[\sum_{l=1}^{L}(\hat{H}_l P_l^T d_l -$$

$$\sum_{l=1}^{L}(\hat{H}_l^T P_l^T P_l(\hat{H}_l g^{(n)})] - a B^T B g^{(n)}\} \qquad (12)$$

The first sum can be pre-calculated and stored as a 3D volume in the computer memory. Thus, the input projections d_l have to be read only once and are never again accessed during the course of the iterations. In addition, the product B^TB is the Laplacian of the 3D volume $g^{(n)}$, which can be calculated more efficiently without actually creating the matrix B^TB. The point spread function is space-invariant, so H_l has a block-Toeplitz structure [2], and H_l is equal to H_l^T. Because of the large size of the matrix it is more convenient to use the CTF H_l in Fourier space and to modify the Fourier transform of the volume instead of using matrix multiplication or real space convolution.

Application to Energy-Filtered Images of the 70S *E. coli* Ribosome

The specimen was prepared following the procedure of Wagenknecht *et al.* [31]. Molybdenum 400-mesh grids were used to minimize thermal effects. The specimens were examined in a Zeiss/LEO EM912 (Oberkochen, Germany) transmission electron microscope operated at 120 kV. The microscope is equipped with a Köhler illumination system and an Omega energy filter. All the microscopy was done at a temperature below -170°C using an Oxford cryo-holder CT3500 (Oxford Instruments, Oxford, UK) and temperature controlling unit. A 90 µm object aperture was used in all experiments. Three images were taken at zero degree tilt of the same specimen area using the defocus settings 1.5 µm, 2.0 µm and 2.5 µm at a magnification of 52000x, which was calibrated using catalase crystals. The dose for each exposure was 5e$^-$/Å^2, thus the total dose accumulation reached 15e$^-$/Å^2 for the data collected at 2.5 µm defocus. The width of the zero-loss energy filter was 14 eV. Images were recorded on Kodak (Rochester, NY) SO163 films and processed in the developer D19 at full strength for 12 minutes. The negatives were scanned using the Perkin Elmer (Norwalk, CT) flatbed PDS 1010A microdensitometer with a step size of 20 µm. The corresponding pixel size on the specimen is 3.8Å.

The parameters of the CTFs (defocus, source size, energy spread, amplitude contrast ratio) were determined using the method described by Zhu *et al.* [33]. Briefly, the power spectrum of a large field is computed and rotationally averaged. The resulting profile is background corrected and fitted on the basis of CTF theory and analytical expressions for the envelope terms. The amplitude contrast ratio was determined as 0.14. After windowing the particles were subjected to the 3D projection alignment procedure [18] with an angle increment of 2°. A previous reconstruction of the 70S ribosome [18] was used as initial reference for a 2.5 µm-defocus group (2254 images). The resulting reconstruction was used as a reference for a 2.0 µm-defocus group (2043 images) and the result was used as a reference for a 1.5 µm-defocus group (1539 images) (Figs. 3a and 3b). Finally, after all the necessary parameters were established, images from all three groups were used in a 3D reconstruction with the CTF compensation program (Figs. 3c and 3d), as described in the section on "Methods of Correction for the CTF". To test the influence of the non-linear constraints on the 3D reconstruction process we decided to use the most intuitive one, namely a positivity constraint. Since the CTF-corrected volume should be linearly related to the Coulomb potential distribution within the object it is reasonable to assume that the density values should be positive. The 3D reconstruction calculated by enforcing positivity of the volume is shown in Figures 3e and 3f.

The gain in resolution after the CTF correction and merging of three defocus groups is easy to notice on the surface representations (Fig. 3d *versus* Fig. 3b), but is particularly striking in the appearance of the central slice (Fig. 3c *versus* Fig. 3a). The number of high-frequency internal details increases dramatically and broad maxima have become better localized. The addition of the positivity
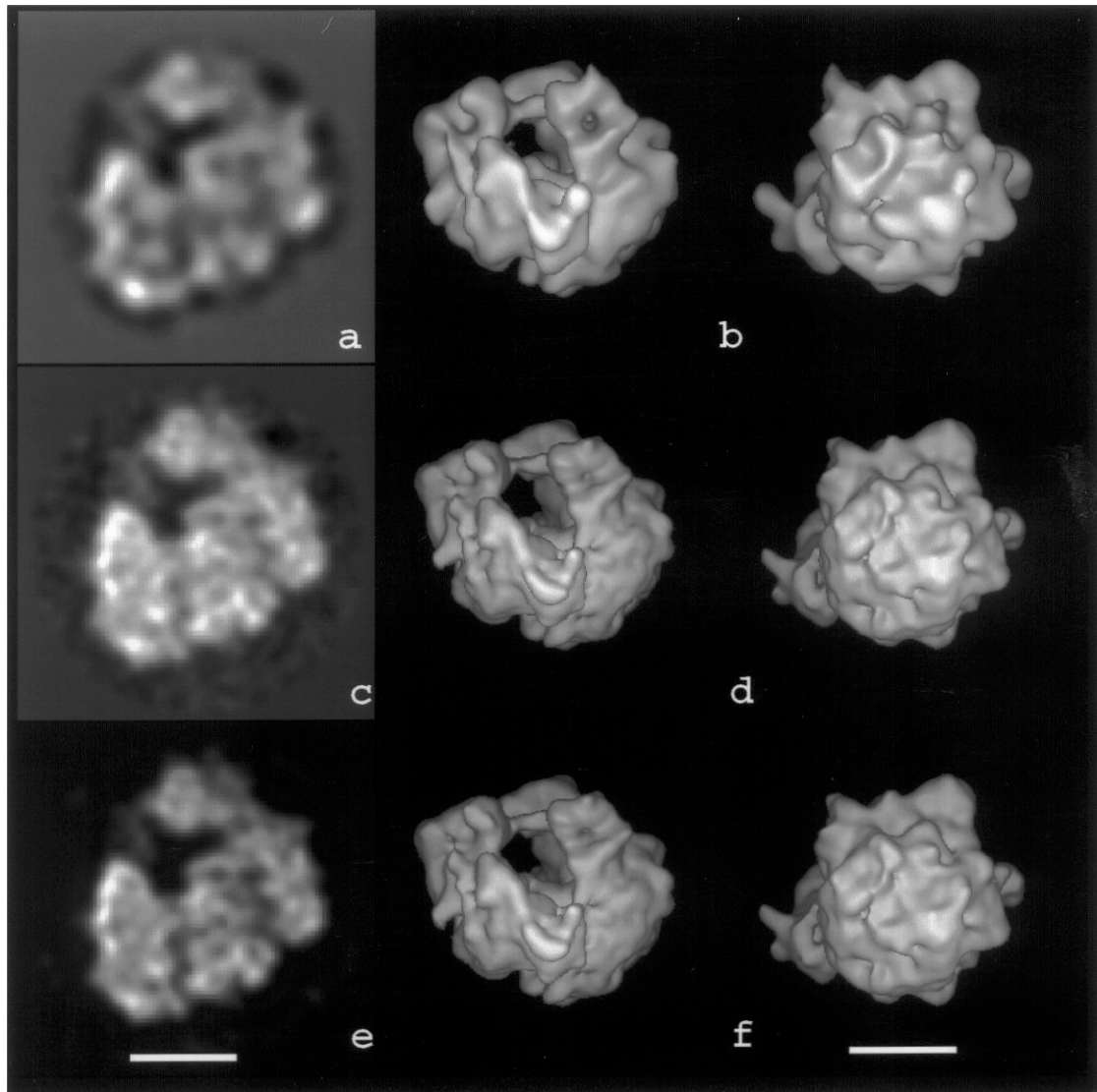
Figure 3. 3D reconstruction of the 70S *E. coli* ribosome. (**a**) Central slice of the 1.5 μm data set reconstruction. (**b**) Surface representations of the 1.5 μm data set reconstruction. (**c**) Central slice of the CTF-corrected reconstruction using three data sets with defocus settings 1.5 μm, 2.0 μm and 2.5 μm, respectively. (**d**) Surface representations of the CTF-corrected reconstruction using three data sets with defocus settings 1.5 μm, 2.0 μm and 2.5 μm, respectively. (**e**) Central slice of the CTF-corrected reconstruction using the positivity constraint and three data sets with defocus settings 1.5 μm, 2.0 μm and 2.5 μm, respectively. (**f**) Surface representations of the CTF-corrected reconstruction using three data sets with defocus settings 1.5 μm, 2.0 μm and 2.5 μm, respectively. Scale bars = 100 Å.

constraint to the 3D reconstruction and CTF correction process does not change the surface representation in any significant way (Fig. 3f *versus* Fig. 3d). The main difference can be noticed in the central slice (Fig. 3e) where the artifacts surrounding the structure are all but eliminated.

The analysis of resolution was done using Fourier Shell Correlation (FSC) curves (FSC is a 3D version of Fourier Ring Correlation measure [23]). For each 3D reconstruction all the input projections were divided randomly into two equal subsets, for each subset a 3D reconstruction was calculated and these two volumes were compared in Fourier space using FSC curves (Fig. 4). The curve for 1.5 μm-defocus data set has a first minimum at approximately $1/25$ $Å^{-1}$, which is the position of the first zero of the corresponding CTF (Fig. 2). The curve for CTF-corrected reconstruction using three data sets with defocus settings

1.5 µm, 2.0 µm and 2.5 µm has a minimum at lower frequency and then rises at 1/25 Å⁻¹, which proves that the gap in frequency range caused by the zero of the CTF was successfully filled by the information originating from two other data sets. The FSC curve for the CTF-corrected reconstruction decreases quickly at about 1/19 Å⁻¹. In this region CTFs for both 2.0 µm and 2.5 µm data sets intersect zero. The CTF for 1.5 µm data set has a maximum in this region, but as it is clear from its FSC curve that SNR is insufficient to provide significant contributions to the merged reconstruction. Thus, due to the particular choice of defocus values there was no phase information recovered past the spatial frequency of 1/20 Å⁻¹. The addition of the positivity constraint modified the FSC significantly. In the whole frequency range considered the FSC has higher values and extends to almost 1/15 Å⁻¹. Nevertheless, the visual analysis of the corresponding structures and, most significantly, the central slices (Figs. 3c and 3e) leads to the conclusion that the gain in resolution is mostly due to the elimination of artifacts in the background, not due to the increase in details of the structure.

The influence of CTF correction on the reconstructed structures is best illustrated on the histogram of density (Fig. 5). The 70S ribosome should have two main density components, namely protein and RNA. In addition, the ice surrounding the structure and filling its cavities and tunnels should have a major contribution. This can be noticed on the corresponding histograms: both 1.5 µm defocus data set and CTF-corrected volume have large maximum in their histogram of mass around the zero value (in the course of the 3D reconstruction process the density of ice was arbitrarily set to zero). The main difference is the position of the second maximum, which in the case of the 1.5 µm reconstruction is hardly separated from the "ice maximum", while after CTF correction the gap between the two maxima becomes wider. The histogram of density of the third reconstruction has a shape similar that of the CTF-corrected: two maxima are separated, but the negative values are eliminated.

Conclusions

The application of the 3D reconstruction with CTF compensation procedure to the energy filtered EM images of 70S *E. coli* ribosome proves that this strategy leads to the significant increase in the resolution (as measured by FSC curves). Due to the availability of the reference volume and application of the 3D projection alignment procedure the results could be obtained in a relatively short time. The FSC curves agree with the resolution limits set by the parameters of CTFs, as estimated from the micrographs using a newly designed retrieval procedure. The particular choice of the defocus settings in the collected defocus series (1.5
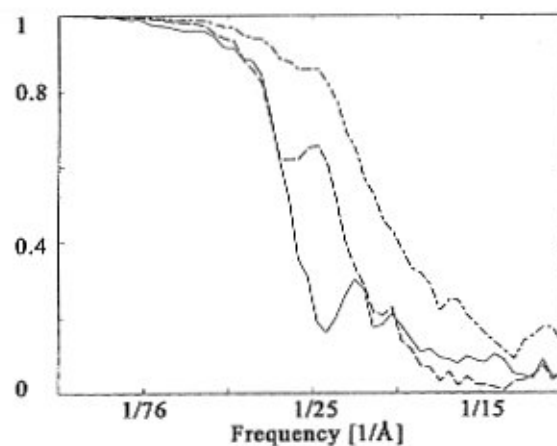

Figure 4. Resolution estimations using Fourier Shell Correlation curves for 1.5 µm (_____), CTF-corrected (-----), and CTF-corrected with positivity constraints (-·--·-) 3D reconstruction of the 70S *E. coli* ribosome.

Figure 5. Histogram of mass distribution for 1.5 µm (_____), CTF-corrected (-----), and CTF-corrected with positivity constraints (-·--·-) 3D reconstruction of the 70S *E. coli* ribosome.
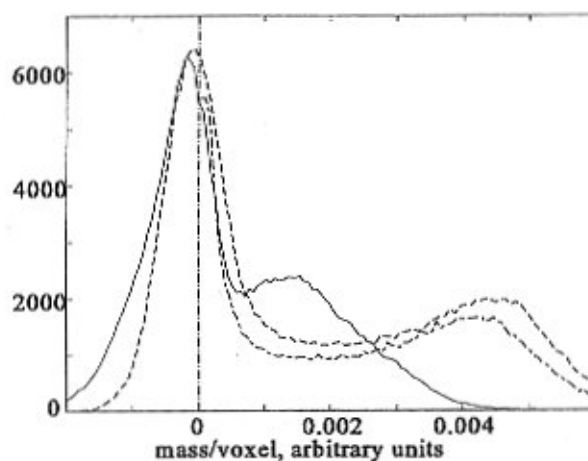
µm, 2.0 µm and 2.5 µm) proved to be the most important factor in the limiting the resolution of the merged, CTF-corrected reconstruction. Further experiments with other choices of defocus settings are necessary to establish the practical limit to the resolution that can be obtained using energy filtered EM data.

Acknowledgements

References

1. Andrews HC, Hunt BR (1977) Digital Image Restoration. Prentice-Hall, Englewood Cliffs, NJ.

2. Biemond J, Lagendijk RL, Mersereau RM (1990) Iterative methods for image deblurring. Proc IEEE **78**: 856-883.

3. Downing KH, Grano DA (1982) Analysis of photographic emulsions for electron microscopy of two-dimensional crystalline specimen. Ultramicroscopy **7**: 381-404.

4. Erickson HP, Klug A (1970) The Fourier transform of an electron micrograph: effects of defocusing and aberrations, and implications for the use of underfocus contrast enhancement. Ber Bunsenges Phys Chem **74**: 1129-1137.

5. Frank J (1969) Nachweis von Objektbewegungen im lichtoptischen Diffraktogramm von elektronenmikroskopischen Aufnahmen (Demonstration of movement of objects in the light optical diffractogram of electron microscopic images). Optik **30**: 171-180.

6. Frank J (1972) A study on heavy/light atom discrimination in bright field electron microscopy using the computer. Biophys J **12**: 484-511.

7. Frank J (1973) The envelope of electron microscopic transfer functions for partially coherent illumination. Optik **38**: 519-536.

8. Frank J, Penczek P, Grassucci R, Srivastava S (1991) Three-dimensional reconstruction of the 70S *Escherichia coli* ribosome in ice - the distribution of ribosomal RNA. J Cell Biol **115**: 597-605.

9. Frank J, Zhu J, Penczek P, Li Y, Srivastava S, Verschoor A, Grassucci R, Lata RK, Agrawal RK (1995) A model of protein synthesis based on cryo-electron microscopy of the *E. coli* ribosome. Nature **376**: 441-444.

10. Frank J, Penczek P (1995) On the correction of the contrast function in biological electron microscopy. Optik **98**: 125-129.

11. Hanszen KH, Trepte L (1971) The contrast transfer function of the electron microscope with partial coherent illumination. Part A: the ring condensor. Optik **33**: 166-181.

12. Hanszen KH, Trepte L (1971) The contrast transfer function of the electron microscope with partial coherent illumination. Part B: disk shape source. Optik **33**: 182-198.

13. Henderson R, Glaeser RM (1985) Quantitative analysis of image contrast in electron micrographs of beam-sensitive crystals. Ultramicroscopy **16**: 139-150.

14. Langmore JP, Smith MF (1992) Quantitative energy-filtered electron microscopy of biological molecules in ice. Ultramicroscopy **46**: 349-373.

15. Lenz F (1971) Transfer of image information in the electron microscope. In: Electron Microscopy in Material Science. Valdrè U (ed). Academic Press, New York. pp 540-568.

16. Lepault J, Booy FP, Dubochet J (1983) Electron microscopy of frozen biological suspensions. J Microsc **129**: 89-102.

17. Penczek P, Radermacher M, Frank J (1992) Three-dimensional reconstruction of single particles embedded in ice. Ultramicroscopy **40**: 33-53.

18. Penczek PA, Grassucci RA, Frank J (1994) The ribosome at improved resolution: new techniques for merging and orientation refinement in 3D cryo-electron microscopy of biological particles. Ultramicroscopy **53**: 251-270.

19. Pratt WK (1991) Digital Image Processing. John Wiley & Sons, Inc., New York.

20. Press WH, Teukolsky SA, Vetterling WT, Flannery BP (1992) Numerical Recipes. Cambridge University Press, Cambridge.

21. Radermacher M, Wagenknecht T, Verschoor A, Frank J (1987) Three-dimensional reconstruction from a single-exposure, random conical tilt series applied to the 50S ribosomal subunit of *Escherichia coli*. J Microsc **146**: 113-136.

22. Reimer L, Ross-Messemer M (1990) Contrast in the electron spectroscopic imaging mode of a TEM. J Microsc **159**: 143-160.

23. Saxton WO, Baumeister W (1982) The correlation averaging of a regularly arranged bacterial envelope protein. J Microsc **127**: 127-138.

24. Schiske P (1973) Image processing using additional statistical information about the object. In: Image Processing and Computer-Aided Design in Electron Optics. Hawkes PW (ed). Academic Press, London. pp 82-90.

25. Schröder RR, Manstein DJ, Jahn W, Holden H, Rayment I, Holmes KC, Spudich JA (1993) Three-dimensional atomic model of F-actin decorated with *Dictyostelium* myosin S1. Nature **364**: 171-174.

26. Smith MF, Langmore JP (1992) Quantitation of molecular densities by cryo-electron microscopy. Determination of the radial density distribution of tobacco mosaic virus. J Mol Biol **226**: 763-774.

27. Typke D, Hegerl R, Kleinz J (1992) Image restoration for biological objects using external TEM control and electronic image recording. Ultramicroscopy **46**: 157-173.

28. van Heel M (1987) Angular reconstitution: a posteriori assignment of projection directions for 3D reconstruction. Ultramicroscopy **21**: 111-124.

29. Wade RH (1992) A brief look at imaging and contrast transfer. Ultramicroscopy **46**: 145-156.

30. Wade RH, Frank J (1977) Electron microscope transfer functions for partially coherent axial illumination and chromatic defocus spread. Optik **49**: 81-92.

31. Wagenknecht T, Grassucci R, Frank J (1988)

Electron microscopy and computer image averaging of ice-embedded large ribosomal subunits from *Escherichia coli*. J Mol Biol **199**: 137-147.

32. Wagenknecht T (1992) Three-dimensional reconstruction of noncrystalline macromolecular assemblies. In: Electron Tomography. Frank J (ed). Plenum, New York. pp. 359-389.

33. Zhu J, Penczek PA, Schröder RR, Frank J (1997) Three-dimensional reconstruction with CTF correction of the 70S *Escherichia coli* ribosome using energy-filtered cryo-electron microscopy. J Struct Biol **118**: 197-219.